Alteration of the *in vivo* nicotinic receptor density in ADNFLE patients: a PET study

F. Picard,[1] D. Bruel,[2] D. Servent,[3] W. Saba,[2] C. Fruchart-Gaillard,[3] M.-A. Schöllhorn-Peyronneau,[2] D. Roumenov,[2] E. Brodtkorb,[4] S. Zuberi,[5] A. Gambardella,[6] B. Steinborn,[7] A. Hufnagel,[8] H. Valette[2] and M. Bottlaender[2]

[1]Department of Neurology, University Hospital and Medical School of Geneva, Switzerland, [2]CEA, Service Hospitalier Frédéric Joliot, DRM/DSV, Orsay, [3]CEA, Département d'Ingénierie et d'Etudes des Protéines, Saclay, France, [4]St Olav's Hospital, Trondheim University Hospital Trondheim, Norway, [5]Royal Hospital for Sick Children, Yorkhill, Glasgow, UK, [6]University Magna Graecia, Catanzaro, Italy, [7]University of Medical Sciences, Poznan, Poland and [8]Department of Neurology, University of Essen, Essen, Germany

Correspondence to: Dr Fabienne Picard, Department of Neurology, University Hospital of Geneva, 24 rue Micheli-du-Crest, 1211 Geneva 14, Switzerland
E-mail: Fabienne.Picard1@hcuge.ch

Nicotinic acetylcholine receptors (nAChRs) are involved in a familial form of frontal lobe epilepsy, autosomal dominant nocturnal frontal lobe epilepsy (ADNFLE). In several ADNFLE families, mutations were identified in the nAChR α4 or β2 subunit, which together compose the main cerebral nAChR. Electrophysiological assessment using *in vitro* expression systems indicated a gain of function of the mutant receptors. However the precise mechanisms by which they contribute to the pathogenesis of a focal epilepsy remain obscure, especially since α4β2 nAChRs are known to be widely distributed within the entire brain. PET study using [^{18}F]-F-A-85380, a high affinity agonist at the α4β2 nAChRs, allows the determination of the regional distribution and density of the nAChRs in healthy volunteers and in ADNFLE patients, thus offering a unique opportunity to investigate some *in vivo* consequences of the molecular defect. We have assessed nAChR distribution in eight non-smoking ADNFLE patients (from five families) bearing an identified mutation in nAChRs and in seven age-matched non-smoking healthy volunteers using PET and [^{18}F]-F-A-85380. Parametric images of volume of distribution (Vd) were generated as the ratio of tissue to plasma radioactivities. The images showed a clear difference in the pattern of the nAChR density in the brains of the patients compared to the healthy volunteers. Vd values revealed a significant increase (between 12 and 21%, $P < 0.05$) in the ADNFLE patients in the mesencephalon, the pons and the cerebellum when compared to control subjects. Statistical parametric mapping (SPM) was then used to better analyse subtle regional differences. This analysis confirmed clear regional differences between patients and controls: patients had increased nAChR density in the epithalamus, ventral mesencephalon and cerebellum, but decreased nAChR density in the right dorsolateral prefrontal region. In five patients who underwent an additional [^{18}F]-fluorodeoxyglucose (FDG) PET experiment, hypometabolism was observed in the neighbouring area of the right orbitofrontal cortex. The demonstration of a regional nAChR density decrease in the prefrontal cortex, despite the known distribution of these receptors throughout the cerebral cortex, is consistent with a focal epilepsy involving the frontal lobe. We also propose that the nAChR density increase in mesencephalon is involved in the pathophysiology of ADNFLE through the role of brainstem ascending cholinergic systems in arousal.

Keywords: ADNFLE; genetics; nicotinic receptor; PET; fluoro-A-85380

Abbreviations: ACh = acetylcholine; ADNFLE = autosomal dominant nocturnal frontal lobe epilepsy; *CHRNA4* = gene coding for the neuronal nicotinic acetylcholine receptor α4 subunit; *CHRNB2* = gene coding for the neuronal nicotinic acetylcholine receptor β2 subunit; F-A-85380 = 2-fluoro-A-85380; FDG = fluorodeoxyglucose; IPN = interpeduncular nucleus; LDT = laterodorsal tegmental nucleus; nAChR = nicotinic acetylcholine receptor; SPM = statistical parametric mapping; Vd = volume of distribution; VOI = volume of interest

Received January 20, 2006. Revised April 30, 2006. Accepted May 15, 2006. Advance Access publication June 30, 2006

Introduction

Nocturnal frontal lobe epilepsy (NFLE) is a common non-lesional focal epilepsy (Provini *et al.*, 1999). It is sometimes familial, with an autosomal dominant mode of inheritance (Scheffer *et al.*, 1995). More than a hundred families with autosomal dominant nocturnal frontal lobe epilepsy (ADNFLE) have been reported since the description of the familial form (Picard and Scheffer, 2005). The pathophysiological mechanisms are probably very similar in the sporadic and the familial forms. Therefore, new insight from studies in ADNFLE may contribute to an increased understanding of the pathways involved in NFLE in general.

ADNFLE was the first idiopathic epilepsy in which a causative gene was found. Mutations were identified in twelve families and in one sporadic case in the *CHRNA4* and the *CHRNB2* genes coding for two different subunits (α4 and β2) of the neuronal nicotinic acetylcholine receptor (nAChR) (Steinlein *et al.*, 1995; Phillips *et al.*, 2000; Bertrand *et al.*, 2005; Picard and Scheffer, 2005). This finding opened the new era of epilepsies considered as channelopathies. However, the discovery of a responsible gene does not imply a prompt understanding of the pathogenesis of the disease. The nAChR α4 and β2 subunits are known to assemble, classically in a 2α/3β ratio, and to form the main brain nicotinic receptor subtype in humans. All identified ADNFLE mutations are located within the M2 or M3 transmembrane segments lining the ionic pore of the receptor. The mutant nAChRs have been electrophysiologically studied *in vitro*. In order to mimic the *in vivo* conditions of an autosomal dominant disease, co-injection in frog oocytes of both the normal and mutant alleles of the mutant gene, in addition to the normal allele of the other subunit, resulted in expression of 'heterozygous' mutant receptors. In these conditions, the only common electrophysiological finding for six studied mutations was a significant increase in sensitivity to acetylcholine (ACh) of the mutant receptors (Moulard *et al.*, 2001; Phillips *et al.*, 2001; Bertrand *et al.*, 2002, 2005; Leniger *et al.*, 2003). Another mutation, the *CHRNB2* V287L mutation, caused a retardation of channel desensitization (De Fusco *et al.*, 2000). Thus, contrary to the first conclusions deduced from the assessment of 'homozygous' mutant receptors (Weiland *et al.*, 1996), the recent studies suggest a gain of function of the mutant nicotinic receptors. As an alternative common mechanism, another study of five mutations suggested a reduction of the Ca^{2+} dependence of the ACh response (Rodrigues-Pinguet *et al.*, 2003).

Although the electrophysiological studies suggest that a gain of function of the mutant receptors may exist *in vivo*, the precise mechanisms behind the epilepsy in ADNFLE remain unknown. The α4β2 nAChRs are widely distributed, in particular in the thalamus and the cortex, yet their precise distribution in the human brain is still incompletely known. Most of these receptors are presynaptic and have a neuromodulatory role consisting of an enhancement of the release of GABA, glutamate, dopamine, norepinephrine, serotonin or ACh. Some receptors that alter the release of various neurotransmitters are axonal at a preterminal location (Lena *et al.*, 1993). The presence of postsynaptic receptors has also been demonstrated; they mediate fast excitatory synaptic transmission (Dani, 2001). Until now, the brain and cellular (pre-, post- or extrasynaptic) localizations of the mutant α4β2 nAChRs directly involved in ADNFLE pathogenesis have not been identified. Although animal models might provide a first insight into the pathogenesis, their results must be interpreted with caution given the differences in brain organization and receptor distribution. A more definitive answer might be obtained with studies of receptor distribution in the living human brain. *In vivo* PET studies may help to understand the link between the molecular alteration, the cellular dysfunction and the clinical expression.

2-[^{18}F]-fluoro-A-85380 ([^{18}F]-F-A-85380) is a PET radiotracer for brain imaging of nAChRs. It has a high affinity for heteromeric nAChRs (mainly represented by the α4β2 receptors). Its *in vivo* characterization has been performed in rodents and in monkeys (Valette *et al.*, 1999*a*, *b*). Its use has been validated in humans in healthy volunteers (Kimes *et al.*, 2003; Gallezot *et al.*, 2005). In the present study, we compared the regional density of nAChRs in a group of ADNFLE patients bearing an identified mutation with that of a group of control subjects, after having checked *in vitro* that the mutations do not change the affinity of the radioligand for the nAChRs. Statistical parametric mapping (SPM) was used to compare group means.

Material and methods

In vitro studies

Materials

cDNA coding for human α4, β2 and α4−S248F were kindly provided by O. Steinlein (University of Munich, School of Medicine, Institute of Human Genetics, Munich, Germany) and β2−V287L by G. Casari (San Raffaele University, Milan, Italy). (±)-[^{3}H]-epibatidine (55.5 Ci/mmol) was purchased from PerkinElmer and carbamazepine from Sigma. cDNA coding for neuronal nicotinic receptor subunits (wild-type and mutant α4 and β2) were transfected into human embryonal kidney (HEK 293) cells by calcium precipitation as described previously (Chen and Okayama, 1987). Briefly, for the wild-type receptor, cDNAs (7 μg α4 + 7 μg β2) were transfected by calcium precipitation with careful control of the pH (6.95). For the mutant receptors, different types of transfection were made in order to simulate a 'heterozygous' (3.5 μg α4 + 3.5 μg α4-S248F + 7 μg β2) or (7 μg α4 + 3.5 μg β2 + 3.5 μg β2-V287L) or a 'homozygous' (7 μg α4-S248F + 7 μg β2) or (7 μg α4 + 7 μg β2-V287L) mutant receptor. The cells were placed at 37°C under 5% CO_2 and 20 h after transfection the medium was changed. Then, the cells were placed for 2 days at 30°C, under 5% CO_2 before collection in a phosphate-buffered saline (PBS) with 5 mM EDTA, washed twice with PBS and finally resuspended in 3 ml/plate of this buffer for the binding experiments.

Competition binding assays

The affinities of epibatidine and F-A-85380 for the different α4β2 constructions were determined by equilibrium binding experiments using [^{3}H]-epibatidine as radioactive tracer. Cells expressing the receptor were incubated with 0.5 nM [^{3}H]-epibatidine and various concentrations of competitive ligands for 2 h. The solution was filtered through GF/C filters, previously soaked in PBS + polyethyleneimine 0.5%, and the filters were washed with 6 ml of cold PBS, dried and counted on a Rackbeta counter (PerkinElmer LAS, Courtaboeuf, France) after the addition of 10 ml of scintillation solution (Lipoluma-PerkinElmer LAS, Courtaboeuf, France).

In equilibrium competition experiments, IC_{50} values were determined by fitting the competition data by the empirical Hill equation and converted to K_i constants using the Cheng–Prussoff equation with K_d value [^{3}H]-epibatidine on human α4β2 of 20 pM.

All experiments were performed at least three times in duplicate to ensure consistency.

Almost all the patients (6/8) were treated with carbamazepine at the time of the study. This drug seems to act on the ionic pore of the nAChRs as an open channel blocker (Picard *et al.*, 1999). An additional effect on the binding site has never been excluded. Therefore, the effect of carbamazepine on the F-A-85380/[^{3}H]-epibatidine binding on both wild-type and mutant receptors was evaluated by measuring the potency of 50 μM of carbamazepine to compete with the radiotracer and by comparing the K_i of F-A-85380 with or without 50 μM of carbamazepine. This concentration is within the presumed therapeutic range (20–50 μM).

Saturation binding assays using [^{18}F]-F-A-85380

Assays were carried out at 37°C in HEPES-salt solution (HSS), containing HEPES (pH 7.4, 15 mM), 120 mM NaCl, 5.4 mM KCl, 0.8 mM MgCl2 and 1.8 mM CaCl. Cells expressing the receptor (10 μl) were incubated for 2 h in a total volume of 2 ml with 0.04 to 33 nM [^{18}F]-F-A-85380. Non-specific binding was determined in the presence of 300 μM (−)-nicotine. Incubation was terminated by filtration through GF/B glass fibre filters, presoaked in 1% polyethyleneimine, using a Brandel 48-channel cell harvester (Inotech-IH-110, PerkinElmer, Courtaboeuf, France). Filters were washed three times with 3 ml aliquots of buffer [50 mM Tris–HCl (pH 7.4)]. Radioactivity was measured using an automatic gamma counter (model 5000; Packard Instrument Co., Downers Grove, IL). Binding parameters were determined from experimental data using a non-linear least squares regression program (GraphPad Prism). All experiments were performed at least three times in triplicate.

In vivo studies

Subjects

Eight non-smoking Caucasian patients with ADNFLE and an identified mutation in the nicotinic receptor (seven men; one woman; mean age = 31 years, SD = 13.2) and seven non-smoking age-matched healthy Caucasian volunteers (seven men; mean age = 35 years, SD = 15.5 ; P = 0.44) were studied. All patients were right-handed.

These patients belong to five families previously reported to harbour mutations in the *CHRNA4* (nAChR α4 subunit) gene or the *CHRNB2* (nAChR β2 subunit) gene. The patients came from Scotland [Family D (McLellan *et al.*, 2003)], Norway (Steinlein *et al.*, 2000), Italy (De Fusco *et al.*, 2000; Gambardella *et al.*, 2000), Poland (Rozycka *et al.*, 2003) and Germany (Leniger *et al.*, 2003). Six patients had mutations in the α4 subunit and two in the β2 subunit. Patient characteristics, including type of mutation, are shown in Table 1.

The usual antiepileptic medication was continued at the time of the PET examination. Three patients were on carbamazepine alone, three patients on carbamazepine plus clonazepam or clobazam (of whom one demonstrated non-compliance with an undetectable plasma level of carbamazepine, <2.5 μg/ml), one patient on oxcarbazepine plus levetiracetam and one on clobazam alone.

Two patients had seizures the night before the [^{18}F]-F-A-85380 PET examination.

Study design

The study protocol for this investigation was approved by the Medical Bioethics Committee of the Medical Centre at the University of Paris XI and written informed consent was obtained from all subjects.

All subjects had a MRI scan and a [^{18}F]-F-A-85380 PET scan on the same day. Neither patients nor controls fell asleep during the PET examination. In addition, five of the patients had a [^{18}F]-fluorodeoxyglucose (FDG) PET on the following day. All PET studies were performed using an ECAT EXACT HR+ tomograph (Siemens Medical Solutions, Knoxville, TN, USA). This tomograph allows simultaneous acquisition in 3D mode of 63 slices with an isotropic intrinsic resolution of 4.5 mm.

Magnetic resonance imaging

MRI scan was performed on a 1.5 tesla signa system (General Electric, Milwaukee, WI). A T_1-weighted inversion-recovery sequence in 3D mode and a 256 × 192 matrix over 124 slices (1.5 mm thick) were used to generate the anatomical images.

[^{18}F]-F-A-85380 PET imaging

A-85380 was labelled with fluorine-18 by no-carrier-added nucleophilic aromatic substitution (Doll *et al.*, 1999). [^{18}F]-F-A-85380 (188 ± 24 MBq, 2–3 nmoles) was injected intravenously. The PET acquisition started 3 h later and lasted 1 h. In five control subjects, the PET acquisition started immediately after tracer injection and lasted 240 min with a rest period between 150 and 210 min (Gallezot *et al.*, 2005). A thermolabile plastic face mask ensured a stable position of the head. Attenuation correction was performed in each individual after segmentation of the attenuation map, using a ^{68}Ge transmission scan acquired for 15 min. Venous plasma samples were drawn and unchanged radiotracer fraction was measured in the plasma using solid phase extraction. Briefly, a 500 μl plasma sample was acidified, directly applied onto a 30 mg Oasis MCX-SPE column and washed with 0.1 N HCl, MeOH and MeOH/H_2O/NH_4OH 50/48/2 (v/v). [^{18}F]-F-A-85380 was eluted twice with a MeOH/NH_4OH 95/5 (v/v) solution. The radioactivity due to unchanged [^{18}F]-F-A-85380 in the eluted fractions was measured in a gamma counter (Cobra Quantum D5003, PerkinElmer, Courtaboeuf, France) (Schöllhorn–Peyronneau *et al.*, 2005).

[^{18}F]-FDG PET imaging

[^{18}F]-FDG was injected intravenously at a mean dose of 148 MBq. Image acquisition started with the injection and lasted

Table 1 Clinical, electrophysiological and neuroimaging edit so it is first patient, the country and patient number on the first line, and the reference, when there is one, below data

Country, patient no.	Norway IV-6 (Steinlein *et al.*, 2000)	Norway IV-3	Scotland IV-1 (Family D, McLellan *et al.*, 2003)	Scotland IV-2	Germany III-2 (Leniger *et al.*, 2003)	Poland III-3 (Rozycka *et al.*, 2003)	Italy III-3 (Gambardella *et al.*, 2000)	Italy III-4
Mutation	α4-S248F	α4-S248F	α4-S248F	α4-S248F	α4-T265I	α4-S252L	β2-V287L	β2-V287L
Sex	M	F	M	M	M	M	M	M
Age, years	45	53	23	20	41	22	23	22
Age at onset, years	13	13	15	12	15	9	11	12
Ictal symptoms	Strange feeling in head, hyperpnoea, hyperkinetic movements	Strange feeling in head, polypnoea, raising of upper part of body, up on knees and elbows, repetitive turning of head	Sitting up, drumming of arms and legs on the bed and gasps for breath	Irregular jerks of upper limbs, staring, falling off the bed	Tonic stiffening of upper limbs, bipedalling of lower limbs, inconsistent talk	Sensation of being out of breath, tonic stiffening, inability to talk	Generalized tingling or shivering or indefinite feeling in head, then grunt or vocalization and dystonic movements of arms	Indefinite feeling in head, then diffuse stiffening followed by truncal flexion and facial grimacing
Ictal breathing difficulty	Yes	Yes	Polypnoea	Polypnoea	No	Yes	No	No
Loss of consciousness	Only at young age	Rare	Yes (wakes up after the seizure and feels unwell)	Yes (wakes up after the seizure and feels unwell)	Yes	No	Yes	Yes
Duration of attacks	<1 min	10–30 s	5–20 s	a few s–1 min	<1 min	10–20 s	10–40 s	10–40 s
Secondary generalization	Only at young age	Rare	No	10 in total	No	Only one after a treatment withdrawal	No	No
Postictal phenomena	Only at young age	No	No	No	No	Motor aphasia (1–2 min); hyperthermia after clusters of seizures	No	No
Time of attacks	Nocturnal (end of night)	Nocturnal	Nocturnal (end of night)	Nocturnal (middle of night)	Nocturnal	Nocturnal (beginning and end of night) and naps	Nocturnal	Nocturnal

No. of seizures per night	3–4	Around 10 (clusters)	Cluster of seizures	Long cluster of seizures (around 20)	4–5	20–30	10–20	1
Interictal EEG	Normal	Normal	Not done	Normal	Sparse bilateral frontotemporal sharp waves, intermittent frontotemporal theta activity	Normal	Sparse bifrontal slow sharp waves	Sparse bifrontal slow sharp waves
Ictal EEG	Arousal with no definite change	Right focal rhythmic abnormalities in some recordings; equivocal in others	Not done	Sudden arousals with high voltage bilateral rhythmic delta waves with superimposed muscle artefact	Not done	Not localizing	Not done	Arousal with no definite change
Brain MRI	Normal	Normal	Normal	Normal	Normal	Normal	Normal	Normal
Current medication	CBZ 800 mg/day and clonazepam 4 mg/day	CBZ 1200 mg/day and clobazam in the evening	CBZ 400 mg/day	CBZ 800 mg/day	Oxcarbazepine 600 mg/day and levetiracetam 2.5 g/day	CBZ 600 mg/day	CBZ 600 mg/day and clobazam 10 mg/day, but no compliance	Clobazam 10 mg/day
Response	Good response with decrease of seizure frequency (1 per month) and milder symptoms these last 15 years	Persistence of seizures ; CBZ stopped the secondary generalizations	Asymptomatic with CBZ (reappearance of seizures when CBZ is stopped)	Persistence of rare seizures (1 or 2 nights per month) related to alcohol, sleep deprivation or CBZ not taken	Persistence of rare seizures (1 or 2 nights with seizures every 2 weeks); poor control even with CBZ 1200 mg/day	Persistence of rare nights with 2–3 seizures (twice a month)	Persistence of 1 seizure/year	Persistence of weekly seizures; refusal of another treatment
Smoker	Never	Yes; stopped 1 year ago	Never	Never	Never	Never	Never	Never
Occurrence of seizures before PET examination	No seizure the previous night	No clear seizure during the preceding nights (short awakenings not excluded)	No (after a seizure, wakes up and feel unwell)	No seizure the previous night (last seizures around 10 days before)	Several seizures the previous night	Three small seizures the previous night	No major seizure the previous night (wakes up when major seizure)	No major seizure the previous night (wakes up when major seizure)

Patient numbers refer to the family trees in the original papers reporting the corresponding families. The Norwegian patients IV-6 and IV-3 were first cousins. The Scottish patients IV-1 and IV-2 were brothers, like the Italian patients III-3 and III-4.
M male; F female; CBZ carbamazepine.

1 h. Reconstructed images were corrected for attenuation using a ^{68}Ge transmission scan.

PET data processing

Parametric images

The data analyses were performed using two approaches: the first is a data-driven analysis based on volumes of interest (VOIs) drawn on the images. Although the VOI technique is a useful method, it only analyses selected areas; thus many brain regions may be left unexplored. The second approach, a voxel-based analysis using the statistical parametric mapping software (SPM2), is expected to overcome this limitation, and the relationship between the change in nAChR density ([^{18}F]-F-A-85380) or in glucose metabolism ([^{18}F]-FDG) and its anatomical basis can be investigated more accurately.

Both data analyses were performed on volume of distribution (Vd) parametric images based on the ratio of brain tissue to unchanged F-A-85380 plasma concentration at equilibrium.

Parametric images were created using Anatomist software (http://brainvisa.free.fr). For each frame collected during the last 30 min of the emission scan, the radioactivity in each voxel was divided by the value of individually metabolite-corrected [^{18}F]-F-A-85380 in venous plasma at the same time, providing thus the Vd for each voxel.

VOI analysis

For all subjects, VOIs were drawn on individual MR T_1 images using Anatomist software (http://brainvisa.free.fr). Cortical VOIs were outlined anatomically, following the grey matter ribbon. The identification of key sulci on individual MR images allowed for the anatomical delineation. To ensure a good reproducibility of the VOI placement, all VOIs were drawn by the same experienced physician.

Fourteen VOIs were delineated in 3D on MR T_1 images, based on clearly identified anatomical structures: prefrontal (31.0 ± 4.6 ml), frontal (9.3 ± 1.1 ml), operculum (3.5 ± 0.5 ml), parietal (8.8 ± 0.5 ml), temporal (6.9 ± 1.2 ml), occipital (10.1 ± 1.7 ml) cortices, caudate nucleus (3.1 ± 0.8 ml), putamen (3.9 ± 0.8 ml), thalamus (5.3 ± 0.9 ml), mesencephalon (1.1 ± 0.1 ml), cerebellum (5.8 ± 1.4 ml), hippocampus (1.6 ± 0.3 ml), pons (1.4 ± 0.4 ml) and corpus callosum (1.6 ± 0.3 ml). The VOI termed 'frontal cortex' corresponded to a grey matter ribbon drawn from the central sulcus on the inferior and middle frontal gyri, and included dorsolateral prefrontal cortex, while the VOI termed 'prefrontal cortex' corresponded to the fronto-polar area of the frontal lobe.

For each VOI, tissue to plasma ratio (Vd) was obtained from the PET parametric images of each subject after co-registration with the corresponding MR images using a mutual information algorithm. In control subjects, the Vd calculated using the tissue to plasma ratios obtained in VOIs were compared with the Vd obtained from kinetic analysis using either a two-tissue compartmental analysis or a Logan graphical analysis as described in Gallezot *et al.* (2005). The Vd obtained in all VOIs in control subjects and patients were compared using a two-way analysis of variance (ANOVA) followed by *post-hoc* *t*-test using the Bonferroni correction (StatView, Abacus Concepts).

SPM analysis of PET images

SPM2 was applied to Vd parametric images to localize mean group differences in [^{18}F]-F-A-85380 uptake between ADNFLE patients and controls on a voxel-by-voxel basis (Wellcome Department of Cognitive Neurology, London, UK; implemented on Matlab 7.2). Prior to statistical analysis, the images were spatially normalized into an appropriate template.

For [^{18}F]-F-A-85380 study, PET scans and MRI of each subject were co-registered. PET images were then normalized into the MRI template (T1.mnc) from SPM2. A smoothing procedure using an isotropic Gaussian kernel of 8 mm in full-width at half maximum was then applied to remove high-frequency noise from the images and to take into account anatomical differences between subjects.

For the [^{18}F]-FDG studies, five ADNFLE patients were compared with a group of 30 control subjects studied at our institution (mean age: 39 years, SD = 15). [^{18}F]-FDG PET images were normalized into a PET-dedicated template. The normalized images were smoothed with a 12 mm Gaussian filter.

For both PET studies, voxel size was 2 × 2 × 2 mm. The SPM comparisons between the parametric images of the patients and the parametric images of the control subjects were performed using a parametric two-sample *t*-test. We evaluated the entire brain volume (>200.000 voxels). For each analysis a proportional voxel threshold of 0.8 and proportional scaling of the parametric images were used. We investigated differences of radiotracer concentrations at an uncorrected P-value < 0.001 and the changes were considered significant at a level of $P < 0.05$ after correction for cluster size. In addition, the significance of some of the voxels constituting the significant clusters was further studied by using a multiple comparison technique.

All indicated coordinates correspond to MNI (Montreal Neurological Institute) coordinates. When precise anatomical localization in the Co-planar Stereotaxic Atlas (Talairach and Tournoux, 1988) was needed, the MNI coordinates of the local maxima of each cluster were converted into Talairach coordinates using an affine transform.

Results

In vitro studies

Competitive interactions between unlabelled and radioactive epibatidine were studied first. The two mutations, α4-S248F and β2-V287L, did not affect the epibatidine affinity for human α4β2 nAChR (data not shown). Thus, identical experimental conditions can be applied in all the competition experiments and the same epibatidine affinity constant can be used for the binding curves. Unlabelled F-A-85380 was able to totally displace [^{3}H]-epibatidine from wild-type and mutant human α4β2 receptors with nearly similar potency (see online Supplementary material, Fig. 1, left panel). The shape of the curves indicates a binding to a single site. The affinity constants (K_i) are reported in Table 2. The mutations α4-S248F or β2-V287L do not modify significantly the affinity of F-A-85380 since values are within the 95% confidence interval (CI) of the measurements. Identical results were obtained whether the transfection simulates a 'heterozygous' or a 'homozygous' profile (data not shown).

Saturation experiments were carried out using the radiotracer [^{18}F]-F-A-85380 itself (see online Supplementary material, Fig. 1, right panel). These experiments allowed direct measurement of the affinity constant (K_D) of F-A-85380 for the receptors. K_D values, reported in Table 2, are very

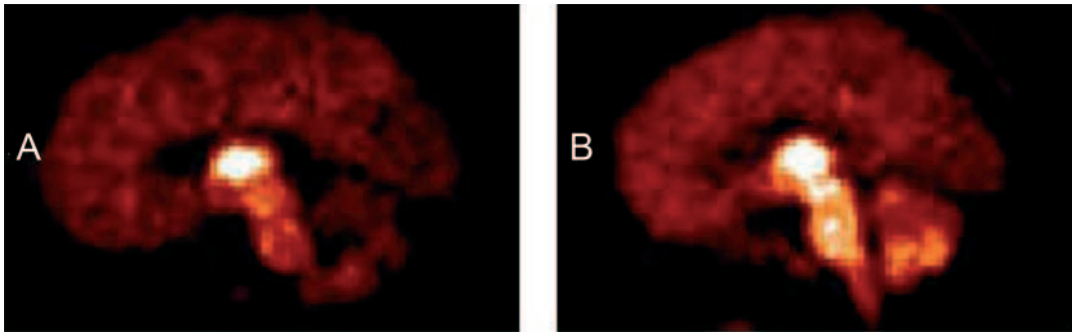

Fig. 1 [^{18}F]-F-A-85380 PET parametric image in one control subject (**A**) and in one ADNFLE patient (**B**).

Table 2 F-A-85380 affinity constants on wild-type and mutant human α4β2 receptors

	K_D (pM) (mean ± SD)	K_i (pM) (mean ± SD)
α4β2	267 ± 84	505 ± 160
α4α4*β2	282 ± 27	780 ± 60
α4β2β2*	265 ± 44	685 ± 130

Affinity constants determined by saturation using [^{18}F]-F-A-85380 (K_D) or by competition using [^{3}H]-epibatidine (K_i). The star (*) indicates a mutated subunit, S248F on α4 and V287L on β2.

close for the wild-type and both mutated receptors, confirming that mutations α4-S248F or β2-V287L do not modify significantly the affinity of F-A-85380.

Carbamazepine (50 μM, approximately the concentration present in the serum of patients treated for epilepsy) did not interfere with the labelled epibatidine and did not modify the F-A-85380 binding either to the wild-type or to the mutant receptors (data not shown).

In vivo studies

[^{18}F]-F-A-85380 VOI analysis

In the seven control subjects, the highest cerebral concentration of the ligand was in the thalamus. High to intermediate levels were observed in the mesencephalon, pons, putamen, caudate nucleus, cerebellum and cortices. The lowest concentration was observed in corpus callosum and occipital cortex. In the eight ADNFLE patients, the distribution of the concentration of ligand had a different pattern: there was a clear increase of the radiotracer uptake in the cerebellum, mesencephalon and pons.

Five of our control subjects belonged to the group of healthy volunteers reported by Gallezot *et al.* (2005). These subjects underwent a long PET protocol allowing kinetic analysis using both a two-tissue compartmental analysis and a Logan graphical analysis. In these control subjects, the comparison between Vd calculated by using these kinetic analyses and the Vd calculated in the present study by using the brain tissue to unchanged F-A-85380 plasma ratio of radioactivities at late time points (4 h after tracer injection) revealed an excellent correlation (identity line, $r = 0.98$, $P < 0.0001$). Therefore, the Vd values calculated by using this ratio did reflect the receptor concentration (Gallezot *et al.*, 2005).

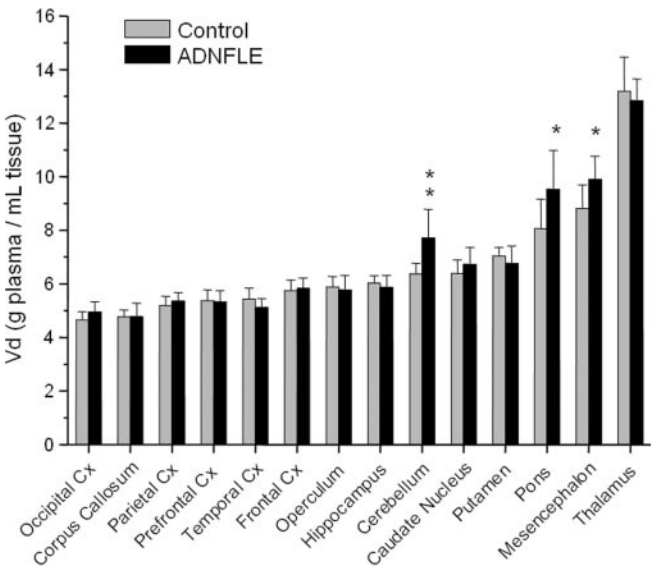

Fig. 2 [^{18}F]-F-A-85380 Vd in the different VOIs, in control subjects ($n = 7$) and ADNFLE patients ($n = 8$). Cx = cortex; *, $P < 0.05$; **, $P < 0.01$ (Bonferroni corrected Student's *t*-test)

The individual parametric images in the patients confirmed the increased fixation in brainstem and cerebellum (e.g. shown in Fig. 1). The comparison of Vd values (Bonferroni corrected Student's *t*-test) in the different VOIs showed a statistically significant increase in the cerebellum, pons and mesencephalon (21%, $P = 0.0078$; 18%, $P = 0.047$ and 12%, $P = 0.035$, respectively) in the group of patients (Fig. 2).

Hyperfixation of [^{18}F]-F-A-85380 detected by SPM analysis

SPM2 was used to compare the voxel values obtained in patients and controls. Increased uptake in the group of patients was tested at uncorrected *P*-values < 0.001. Among the regions with a significant increased uptake, only those

Table 3 SPM analysis of [^{18}F]-F-A-85380 hyperfixation in ADNFLE patients

Location	Local maxima MNI coordinates			*Z*-score (voxel level)	Cluster size (voxels)	$P_{corrected}$ (cluster level)
	x (mm)	*y* (mm)	*z* (mm)			
Mesencephalon	−2	−22	0	4.63	699	< 0.001
	0	−16	−16	4.25		
Left cerebellum	−16	−80	−52	4.21	1256	< 0.001
Right cerebellum	22	−76	−60	4.15	392	0.003
Cerebellar vermis	0	−68	−12	3.94	325	0.007

Patients $n = 8$; controls $n = 7$; $P_{uncorrected} < 0.001$. Regions with a significant increase ($P_{corrected}$ at cluster level < 0.05) are shown. For each cluster, at most three local maxima, separated by at least 8 mm, are given.

providing a *P* corrected for the cluster level < 0.05 were kept. The cluster size threshold allows to select regions that show significant extent of activity. In our study, this threshold, that depends on image characteristics, such as size and smoothness, corresponded to a cluster size of ~300 voxels (2.4 cm^3).

A significant increase of tracer concentration in the group of patients was observed in the region of the mesencephalon and in the cerebellum (Table 3 and Fig. 3).

A cluster of 699 voxels appeared in the region of the mesencephalon (*P* corrected < 0.001 at cluster level). The voxel with the highest *Z*-score (MNI coordinates: −2 −22 0; $Z = 4.63$) was located above the superior colliculi, median, in the superior area of the epithalamus, fitting best with the region of the posterior commissure and habenula (Fig. 3). In this cluster, a second local maximum (MNI coordinates: 0 −16 −16; $Z = 4.25$) was in the lower part of the ventral mesencephalon, in the midline, centred on the interpeduncular nucleus (IPN) according to the Talairach atlas. To identify if the local maxima within this significant cluster were significant at the voxel level, we used *P*-values corrected for multiple comparison. Multiple comparison testing was performed with false discovery rate (FDR) technique (Genovese *et al.*, 2002). We did not report voxel level *P*-values corrected for family-wise error (FWE), as these values were not significant. The lack of effectiveness of this procedure could be related to the extent of our analysis to the entire brain and to the small number of degrees of freedom ($n = 13$). The FDR-correction procedure depends less on the extent of the space of research and applies commonly in SPM. The two above-mentioned local maxima had a *P*-value corrected for FDR at 0.061, which is close to significance. The probability that they corresponded to false positives was thus very low. So the hyperfixation was statistically significant in these voxels, which are located one within the area of the epithalamus (habenular region), the other within the IPN.

The second region with a significant increase was the cerebellum, with three clusters, in the grey matter of the lower part of both cerebellar hemispheres and in the vermis. The voxels with the highest *Z*-scores were in the left hemisphere ($Z = 4.21$; MNI coordinates: −16 −80 −52), part of a cluster of 1256 voxels, and in the right hemisphere ($Z = 4.15$; MNI coordinates: 22 −76 −60), part of a cluster of 392 voxels.

In a second step, SPM analysis was applied to the data of the subgroup of patients with an α4 mutation ($n = 6$) and of the small subgroup of patients with a β2 mutation ($n = 2$). The α4 subgroup showed the same pattern of increased fixation as the whole group of ADNFLE patients, but without significance after correction for cluster size in the mesencephalon (borderline significance at the voxel level for the local maximum located in the lower part of the mesencephalon, at 2 −16 −14, with a $P_{FDR\text{-}corrected} = 0.050$). The β2 subgroup showed a significant increase of tracer concentration at the cluster level in cerebellar hemispheres ($P_{corrected} < 0.0001$). In addition, within a small non-significant cluster appearing in the thalami, there were two local maxima (MNI coordinates: −4 −14 12 and 4 −12 12) with a $P_{FDR\text{-}corrected}$ close to significance ($P = 0.056$), located in the mediodorsal thalamic nucleus, according to the Talairach atlas. Interestingly one of the patients with an α4 mutation (Patient IV-6, Norway) also showed an identical spot (MNI coordinates: −2 −14 10) with a statistically significant *P* at voxel level after correction for FDR, $P_{FDR\text{-}corrected} = 0.035$.

Hypofixation of [^{18}F]-F-A-85380 detected by SPM analysis

In the same way, SPM2 was used to localize any significant cluster of F-A-85380 decreased binding in the group of patients at a $P_{uncorrected} < 0.001$ and a $P_{corrected}$ for the cluster level < 0.05. The cluster size threshold allowing to select regions with significant *P*-values was 200 voxels (1.6 cm^3).

A cluster of 615 voxels was observed in the right prefrontal area ($P_{corrected}$ for the cluster < 0.001). The voxel with the highest *Z*-score was located in the superior frontal gyrus at the border between Brodmann's areas 9 and 10 (MNI coordinates: 28 52 26; $Z = 4.53$; $P_{FDR\text{-}corrected} = 0.081$) (Table 4 and Fig. 4A and B). Other significant clusters were: in the right caudate nucleus (279 voxels; $P_{corrected} = 0.014$; MNI coordinates of the local maximum: 18 24 0; $Z = 3.90$) and in the right rolandic opercular area (215 voxels; $P_{corrected} = 0.041$; MNI coordinates of the local maximum: 56 −4 −2; $Z = 3.86$).

Even at the level of individual patients, the decrease in tracer concentration was statistically significant in the right prefrontal region in seven patients (dorsolateral in three,

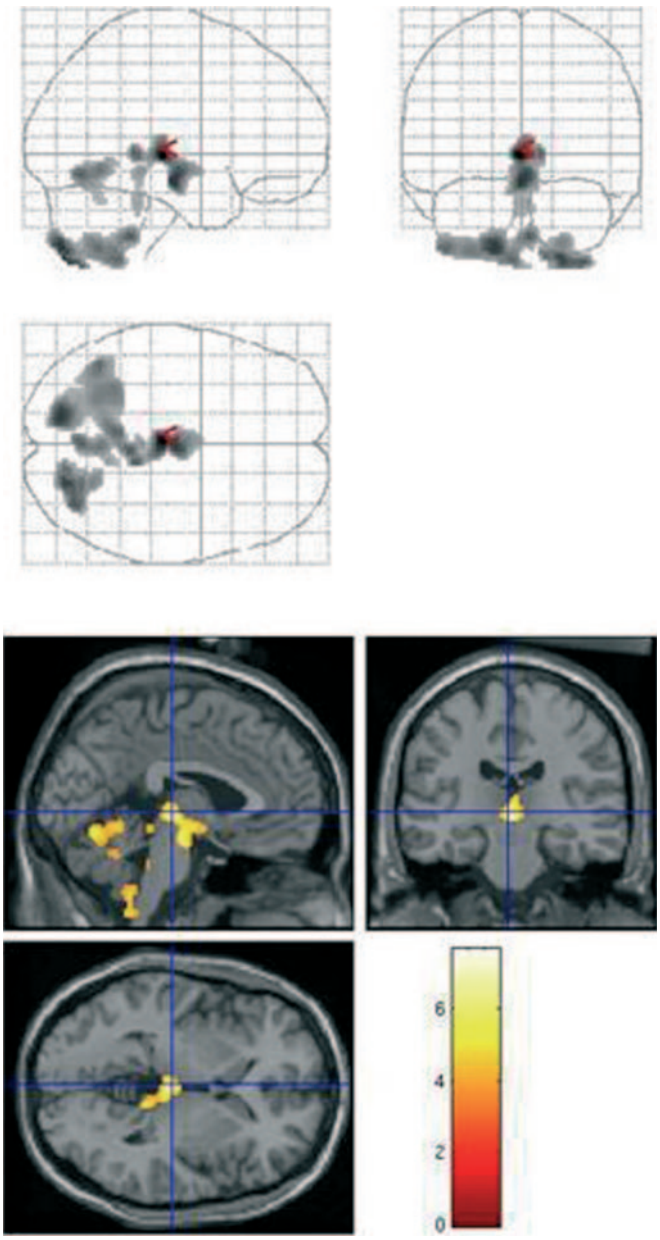

Fig. 3 SPM analysis of [^{18}F]-F-A-85380 hyperfixation in ADNFLE patients (patients $n = 8$; controls $n = 7$; $P_{uncorrected} < 0.001$, $P_{corrected}$ at cluster level < 0.05). These images focus on the mesencephalic cluster (cluster of 699 voxels), with the blue cross centred on the voxel with the highest Z-score ($Z = 4.63$; MNI coordinates: −2 −22 0). This voxel is very median, located above the superior colliculi, in the epithalamus (region of the habenula). The cluster extends in the ventral mesencephalon. Z-values of statistical significance are represented by the colour bar on the right.

orbitofrontal in three and both areas in one patient). A decrease was also observed in the rolandic opercular region (right in seven and left in one) in the eight patients, at a significant level for three patients.

There was no difference between the patients with an α4 mutation and those with a β2 mutation.

SPM analysis of [^{18}F]-FDG PET

FDG PET was carried out in five ADNFLE patients. The SPM comparison was done with a group of 30 healthy volunteers. ADNFLE patients did not show any hyperfixation when compared to controls. A decrease of FDG fixation was observed in the right and left anterior orbitofrontal cortex, with a right predominance, in the right and left opercular regions, and in the right supramarginal gyrus (inferior parietal lobule) in patients (Table 5). However, for all regions, the *P*-values after correction for cluster size were not statistically significant.

The region of the [^{18}F]-F-A-85380 hypofixation and the region of glucose hypometabolism in the right prefrontal cortex were close to each other. The glucose hypometabolism was slightly below the region of [^{18}F]-F-A-85380 hypofixation (Fig. 4A and D). In addition, a concomitant decrease of [^{18}F]-F-A-85380 fixation and glucose metabolism was observed in almost identical parts of the right rolandic opercular region (Fig. 4C and F).

Discussion

The comparison of [^{18}F]-F-A-85380 binding between a group of eight non-smoking ADNFLE patients, in whom a mutation was identified, and a group of control subjects showed clear regional differences. First, the comparison of the parametric PET images between the two groups showed statistically significant increases of tracer fixation in the cerebellum, pons and mesencephalon. The other VOIs showed no significant changes. Second, SPM analysis allowed a more discriminative spatial comparison of the entire brain. A statistically significant increase in nAChR density was observed in the group of ADNFLE patients in a region including the mesencephalon and an adjacent part of the diencephalon (superior area of the epithalamus), and in the cerebellum. Thus, both methods could identify statistically significant changes in mesencephalon and cerebellum. The increase in nAChR density in the brainstem is an exciting discovery which may open new vistas on the pathogenesis of ADNFLE. Moreover, SPM analysis allowed to identify a statistically significant decrease in nAChR density in the right prefrontal area in the group of ADNFLE patients. So far, it has been hard to understand why mutations in receptors that are present in the entire brain result in the clinical picture of a focal epilepsy. This finding of regional decrease in nAChR density may in part explain this phenomenon. The location of the decrease in the prefrontal cortex appears compatible with a frontal lobe epilepsy.

Relevance of the differences observed between ADNFLE patients and control subjects

The nAChR distribution in our group of control subjects agreed with a previous study in non-smoking healthy volunteers using the same tracer (Kimes *et al.*, 2003). This

Table 4 SPM analysis of [^{18}F]-F-A-85380 hypofixation in ADNFLE patients

Location	Local maxima MNI coordinates			*Z*-score (voxel level)	Cluster size (voxels)	$P_{corrected}$ (cluster level)
	x (mm)	*y* (mm)	*z* (mm)			
Right prefrontal cortex	28	52	26	4.53	615	< 0.001
	26	66	12	4.26		
	18	70	6	4.26		
Right caudate	18	24	0	3.90	279	0.014
	26	12	18	3.85		
	26	24	10	3.56		
Right opercular area	56	−4	−2	3.86	215	0.041
	64	−10	−2	3.81		
	56	−14	18	3.81		

Patients $n = 8$; controls $n = 7$; $P_{uncorrected} < 0.001$. Regions with a significant reduction ($P_{corrected}$ at cluster level < 0.05) are shown. For each cluster, at most three local maxima, separated by at least 8 mm, are given.

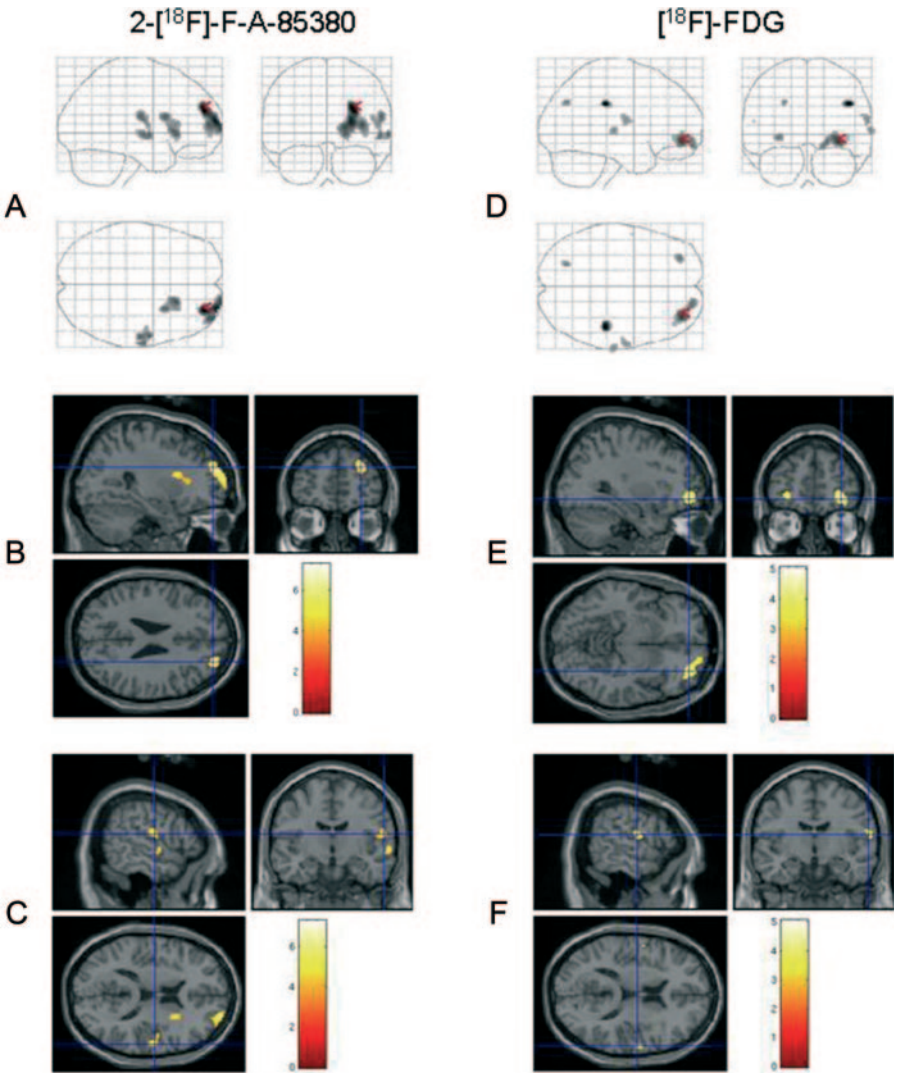

Fig. 4 SPM analysis of [^{18}F]-F-A-85380 and of [^{18}F]-FDG PET hypofixation in ADNFLE patients. (**A–C**) correspond to the [^{18}F]-F-A-85380 analysis (patients $n = 8$; controls $n = 7$; $P_{uncorrected} < 0.001$, $P_{corrected}$ at cluster level < 0.05). (**D**–**F**) correspond to the [^{18}F]-FDG analysis (patients $n = 5$; controls $n = 30$; $P_{uncorrected} < 0.001$). *Z*-values of statistical significance are represented by the colour bar on the right. The figure focuses on the prefrontal region (**B** and **E**) with the region of glucose hypometabolism (**E**) being beneath the region of F-A-85380 hypofixation (**B**). The right side is on the right on the coronal MRI images. Parts **C** and **F** show that the regions of glucose hypometabolism and of F-A-85380 hypofixation in the right opercular cortex are superimposable.

Table 5 SPM analysis of [^{18}F]-FDG PET hypofixation in ADNFLE patients

Location	Local maxima MNI coordinates			*Z*-score (voxel level)	Cluster size (voxels)
	x (mm)	*y* (mm)	*z* (mm)		
Right parietal area	44	−30	32	4.32	71
Right prefrontal cortex	32	50	−8	3.89	329
Left prefrontal cortex	−30	48	−4	3.52	43
Right opercular area	66	−20	4	3.40	34
	64	−8	16	3.38	41
Left opercular area	−56	−2	14	3.11	1

Patients $n = 5$; controls $n = 30$; $P_{uncorrected} < 0.001$.

distribution was also consistent with data obtained *in vitro*, except for the hippocampus which *in vivo* has a slightly higher binding than the neocortex (Marutle *et al.*, 1998).

Before interpreting the alterations of nAChR binding observed in patients, we excluded a bias related to a modification of affinity of the tracer for the nAChRs by either the mutation or the antiepileptic drug carbamazepine.

The affinity of F-A-85380 was determined *in vitro* by two different approaches: indirect affinity measurement (K_i) by competition of F-A-85380 with [^{3}H]epibatidine and direct measurement (K_D) by saturation experiments using the radiotracer [^{18}F]-F-A-85380 itself. Our results showed that, despite the slight difference observed in the K_i values, the affinity (K_D) of the radiotracer [^{18}F]-F-A-85380 was similar for wild-type α4β2 nAChRs and for the mutant α4β2 nAChRs. In the literature, affinity of radioligands for mutant nAChRs was found unchanged (Rodrigues–Pinguet *et al.*, 2003), slightly increased (Fonck *et al.*, 2005) or decreased (Kuryatov *et al.*, 2005).

In addition, oral carbamazepine does not modify the F-A-85380 binding to wild-type or to mutant nAChRs. Indeed, two of our patients who did not take carbamazepine had the same Vd values as patients taking carbamazepine. Also *in vitro*, carbamazepine at a concentration in the therapeutic range did not change the affinity of F-A-85380 for wild-type and mutant α4β2 nAChRs.

nAChR subtype-specificity of [^{18}F]-F-A-85380

The increase of [^{18}F]-F-A-85380 Vd reflects an increased number of heteromeric nAChRs as this tracer has very low affinity for the homomeric α7 subtypes (Deuther–Conrad *et al.*, 2004). Among the heteromeric nAChRs, [^{18}F]-F-A-85380 exhibits a clear selectivity for α4β2 over α3β4 receptors (K_i ratio 1200) (Deuther–Conrad *et al.*, 2004). Affinity of our tracer for the other less abundant subtypes (α3β2, α2β2 and α6β2) remains to be established.

Which mechanisms may give rise to a regional increase in nAChR density?

The mechanisms behind the regional increase in nAChRs in ADNFLE patients are yet unknown. A first possibility is that the mutant nAChRs may have caused regional structural CNS developmental abnormalities. The involvement of the nAChRs in the development of the CNS has been extensively described (Court *et al.*, 1995; Zoli *et al.*, 1995; Adams, 2003; Torrao *et al.*, 2003). The mutant receptors may possibly have allowed the persistence of an excessive number of synapses in the epithalamus, IPN and cerebellum.

A second possibility is a regional upregulation of receptors. In rat, nicotine selectively upregulates α4β2 nAChRs, with a different sensitivity to upregulation in different brain regions (Nguyen *et al.*, 2003). Even choline upregulates the nAChRs (Sallette *et al.*, 2005). In HEK cells expressing the α4-S247F mutant, ACh produced an upregulation of mutant nAChRs (Kuryatov *et al.*, 2005). We postulate that a regional upregulation in the habenulointerpeduncular region in ADNFLE patients could be related to the richness in sites of ACh release and in heteromeric nAChRs in this region (Sastry, 1978; Tribollet *et al.*, 2004; Zoli *et al.*, 1998) and to the hypersensitivity of the ADNFLE mutant nAChRs to ACh.

Could the nAChR density changes be involved in the pathogenesis of ADNFLE?

The regional increases in nAChR density observed in the ADNFLE patients do not seem to be caused by epileptic seizures, since the majority of the patients did not suffer from recent seizures at the time of examination (see Table 1). Larger studies in the future with different populations of patients with epilepsy will determine whether the changes in regional density are specific for the ADNFLE syndrome. If we suppose that these changes indeed are specific, three main questions emerge. Are the regional increases in nAChR density responsible for the sleep-related expression of the disorder? Are these modifications responsible for epileptic seizures? And finally, are they responsible for the particular hypermotor semiology of the seizures?

Are the nAChR density modifications responsible for the sleep-related occurrence of the attacks?

ADNFLE seizures mainly occur during stage 2 of non-rapid eye movement (non-REM) sleep. This stage is characterized by the presence of sleep spindles, which are transient

physiological rhythmic oscillations, with frequencies between 11 and 15 Hz, grouped in sequences that last 0.5–3 s and recur every 3–10 s. They originate in the thalamus and represent thalamocortical oscillations. ADNFLE seizures often seem to arise from sleep spindles (Picard and Scheffer, 2005).

The finding of an increased number of nAChRs in the regions of the epithalamus (medial habenular area) and of the IPN seems particularly interesting in the context of a sleep disorder. These structures are part of the limbic system outflow into the brainstem (Nauta, 1958). They are linked by the fasciculus retroflexus, a cholinergic projection from the medial habenula to the IPN. Interestingly, this tract undergoes an extraordinarily selective degeneration under continuous nicotine exposure in rats (Carlson *et al.*, 2000). The IPN projects to the ventral tegmental area and to reticular and tegmental brainstem nuclei, particularly the laterodorsal tegmental nucleus (LDT), which is part of the ascending cholinergic reticular activating system, involved in arousal regulation (Groenewegen *et al.*, 1986; Smith *et al.*, 1988). This nucleus has important projections to the mediodorsal thalamic nucleus, which projects to prefrontal cortex (Cornwall *et al.*, 1990).

The disruption of the fasciculus retroflexus was shown to alter non-REM sleep duration (Haun *et al.*, 1992). This tract also controls the integrity of REM sleep (Valjakka *et al.*, 1998). Interestingly, metabolism in the IPN is not diminished in non-REM sleep as it is in other brain regions (Kennedy *et al.*, 1982). The IPN could be implicated in the sleep/wake cycle primarily through its connections with the LDT, which during non-REM sleep releases ACh in the thalamus at the time of an arousal. This ACh release triggers an activated awake state in thalamocortical systems (Steriade *et al.*, 1990; Jones, 1993; Williams *et al.*, 1994). Thus, an alteration affecting the IPN could result in arousal disorders.

Could the regional modifications in nAChR density be responsible for epileptic seizures?

The increase in nAChR density in the group of patients affects the habenular region, the IPN, the cerebellum and in three patients the mediodorsal thalamic nucleus at a statistically non-significant level. Except for the cerebellum, we consider that these regions could be involved in pathogenesis of seizures in ADNFLE.

The physiological richness in nAChRs of habenula and IPN, well known in rodents, probably correlates with a high level of sites of ACh release. In IPN, beside postsynaptic nAChRs and presynaptic nAChRs facilitating the release of ACh and of glutamate (Takagi, 1984; Girod and Role, 2001; Grady *et al.*, 2001), other nAChRs are localized at a preterminal level on axons of intrinsic GABAergic neurons (Lena *et al*, 1993). When ACh accumulates extrasynaptically after periods of intense synaptic activity, these preterminal nAChRs may be activated and then prevent prolonged depolarizations of the postsynaptic neurons. In the presence of hypersensitive mutant nAChRs, a low level of ACh or choline could strongly activate postsynaptic receptors, but be insufficient to reach the preterminal receptors, allowing prolonged depolarizations in IPN neurons and in turn overactivation of the LDT.

During the non-REM sleep, when the LDT nucleus, in association with the pedunculopontine nucleus, releases ACh in the thalamus, a tonic activation (desynchronized awake state) is triggered and maintained in the thalamocortical system. *In vivo* electrical stimulation of these nuclei or local application of ACh on thalamocortical neurons induces a depolarization of thalamocortical neurons, first mediated by nicotinic receptors, which interrupts the sleep spindle oscillations (Curro Dossi *et al.*, 1991; Lee and McCormick, 1997).

In ADNFLE, the hyperfunctioning mesopontine cholinergic pathway would chronically overactivate the LDT and consequently the mediodorsal thalamic nucleus. At the time of arousals, the release of ACh in a sensitized mediodorsal thalamic nucleus could prevent the normal arousal-induced interruption of the sleep spindle oscillations and transform them into pathological thalamocortical oscillations, triggering epileptic seizures. Such a transformation of the sleep spindles into epileptic discharges was proposed many years ago in absence epilepsy based on animal models, e.g. the feline generalized penicillin epilepsy (Gloor *et al.*, 1979; Gloor and Fariello, 1988) and the genetic model genetic absence epilepsy rats from Strasbourg (GAERS) (Avanzini *et al.*, 2000), but never in a focal epilepsy.

Could the regional modifications in nAChR density be responsible for the particular hypermotor expression of the seizures?

In ADNFLE, the transformation of the thalamocortical sleep oscillations into pathological oscillations would affect the regions of projection of the mediodorsal thalamic nucleus, namely the orbital and dorsolateral prefrontal cortex, the anterior cingulate cortex and the anterior part of the insula (Behrens *et al.*, 2003; Giguere and Goldman-Rakic, 1988). Interestingly, the frontal sleep spindles, from which the ADNFLE seizures seem to arise, are maximal in cortical regions (Brodmann's areas 9 and 10) which are reciprocally connected to the mediodorsal thalamic nucleus (Anderer *et al.*, 2001).

The decrease in nAChR density and in glucose metabolism observed in the right prefrontal cortex in the group of patients may reflect a neuronal loss, either affecting the prefrontal thalamocortical neurons (presynaptic nAChRs) which undergo an overactivation, or affecting prefrontal cortical neurons (postsynaptic nAChRs) in relation to the epileptic seizures. According to our results, the right rolandic opercular region is involved in the epileptogenic thalamocortical network.

ADNFLE seizures present with intense agitation (frantic and/or dystonic movements) evoking an innate stereotyped motor behaviour of extrapyramidal character. Its precise anatomical origin is not fully understood. The seizures could trigger the release from cortical inhibitory influences of brainstem 'central pattern generators' which control innate motor behaviours essential for survival (Tassinari *et al.*, 2003). Such a disruption of an inhibitory connection from prefrontal regions to the amygdala was recently suggested to account for the release of archaic behaviour suggestive of intense fear in patients with frontal lobe seizures (Bartolomei *et al.*, 2005). In our patients, the prefrontal regions showing a decrease in nAChR density and in glucose metabolism could be implicated in the ictal archaic motor behaviour via a disinhibition of subcortical structures, e.g. at a limbic or extrapyramidal level.

In summary our work shows significant regional changes in brain nAChR density in ADNFLE patients. These changes point towards an overactivated cholinergic pathway ascending from the brainstem. Complementary studies in humans and in animal models are in progress and may help to support the implication of the cholinergic projections from the brainstem to the thalamus in ADNFLE pathogenesis.

Supplementary material

Supplementary data are available at *Brain* Online.

Acknowledgements

This work was supported by the Swiss National Foundation no. 3100A0-104190/1, the DRRC-Assistance Publique des Hôpitaux de Paris, and Sanofi-Aventis. We thank Prof. C. Marescaux, Dr J.-B. Poline and Dr Alexis Roche for helpful discussions and Dr B. Zifkin for critical reading of the manuscript.

References

Adams CE. Comparison of alpha7 nicotinic acetylcholine receptor development in the hippocampal formation of C3H and DBA/2 mice. Brain Res Dev Brain Res 2003; 143: 137–49.

Anderer P, Klosch G, Gruber G, Trenker E, Pascual-Marqui RD, Zeitlhofer J, et al. Low-resolution brain electromagnetic tomography revealed simultaneously active frontal and parietal sleep spindle sources in the human cortex. Neuroscience 2001; 103: 581–92.

Avanzini G, Panzica F, de Curtis M. The role of the thalamus in vigilance and epileptogenic mechanisms. Clin Neurophysiol 2000; 111 (Suppl. 2): S19–26.

Bartolomei F, Trebuchon A, Gavaret M, Regis J, Wendling F, Chauvel P. Acute alteration of emotional behaviour in epileptic seizures is related to transient desynchrony in emotion-regulation networks. Clin Neurophysiol 2005; 116: 2473–9.

Behrens TE, Johansen-Berg H, Woolrich MW, Smith SM, Wheeler-Kingshott CA, Boulby PA, et al. Non-invasive mapping of connections between human thalamus and cortex using diffusion imaging. Nat Neurosci 2003; 6: 750–7.

Bertrand D, Picard F, Le Hellard S, Weiland S, Favre I, Phillips H, et al. How mutations in the nAChRs can cause ADNFLE epilepsy. Epilepsia 2002; 43 (Suppl. 5): 112–22.

Bertrand D, Elmslie F, Hughes E, Trounce J, Sander T, Bertrand S, et al. The CHRNB2 mutation I312M is associated with epilepsy and distinct memory deficits. Neurobiol Dis 2005; 20: 799–804.

Carlson J, Armstrong B, Switzer RC 3rd, Ellison G. Selective neurotoxic effects of nicotine on axons in fasciculus retroflexus further support evidence that this a weak link in brain across multiple drugs of abuse. Neuropharmacology 2000; 39: 2792–8.

Chen C, Okayama H. High-efficiency transformation of mammalian cells by plasmid DNA. Mol Cell Biol 1987; 7: 2745–52.

Cornwall J, Cooper JD, Phillipson OT. Afferent and efferent connections of the laterodorsal tegmental nucleus in the rat. Brain Res Bull 1990; 25: 271–84.

Court JA, Perry EK, Spurden D, Griffiths M, Kerwin JM, Morris CM, et al. The role of the cholinergic system in the development of the human cerebellum. Brain Res Dev Brain Res 1995; 90: 159–67.

Curro Dossi R, Pare D, Steriade M. Short-lasting nicotinic and long-lasting muscarinic depolarizing responses of thalamocortical neurons to stimulation of mesopontine cholinergic nuclei. J Neurophysiol 1991; 65: 393–406.

Dani JA. Overview of nicotinic receptors and their roles in the central nervous system. Biol Psychiatry 2001; 49: 166–74.

De Fusco M, Becchetti A, Patrignani A, Annesi G, Gambardella A, Quattrone A, et al. The nicotinic receptor beta 2 subunit is mutant in nocturnal frontal lobe epilepsy. Nat Genet 2000; 26: 275–6.

Deuther-Conrad W, Patt JT, Feuerbach D, Wegner F, Brust P, Steinbach J. Norchloro-fluoro-homoepibatidine: specificity to neuronal nicotinic acetylcholine receptor subtypes in vitro. Farmaco 2004; 59: 785–92.

Doll F, Dolci L, Valette H, Hinnen F, Vaufrey F, Guenther I, et al. Synthesis and nicotinic acetylcholine receptor in vivo binding properties of 2-fluoro-3-[2(S)-2-azetidinylmethoxy]pyridine: a new positron emission tomography ligand for nicotinic receptors. J Med Chem 1999; 42: 2251–9.

Fonck C, Cohen BN, Nashmi R, Whiteaker P, Wagenaar DA, Rodrigues-Pinguet N, et al. Novel seizure phenotype and sleep disruptions in knock-in mice with hypersensitive alpha4* nicotinic receptors. J Neurosci 2005; 25: 11396–411.

Gallezot JD, Bottlaender M, Gregoire MC, Roumenov D, Deverre JR, Coulon C, et al. In vivo imaging of human cerebral nicotinic acetylcholine receptors with 2-18F-fluoro-A-85380 and PET. J Nucl Med 2005; 46: 240–7.

Gambardella A, Annesi G, De Fusco M, Patrignani A, Aguglia U, Annesi F, et al. A new locus for autosomal dominant nocturnal frontal lobe epilepsy maps to chromosome 1. Neurology 2000; 55: 1467–71.

Genovese CR, Lazar NA, Nichols T. Thresholding of statistical maps in functional neuroimaging using the false discovery rate. Neuroimage 2002; 15: 870–8.

Giguere M, Goldman-Rakic PS. Mediodorsal nucleus: areal, laminar and tangential distribution of afferents and efferents in the frontal lobe of rhesus monkeys. J Comp Neurol 1988; 277: 195–213.

Girod R, Role LW. Long-lasting enhancement of glutamatergic synaptic transmission by acetylcholine contrasts with response adaptation after exposure to low-level nicotine. J Neurosci 2001; 21: 5182–90.

Gloor P, Fariello RG. Generalized epilepsy: some of its cellular mechanisms differ from those of focal epilepsy. Trends Neurosci 1988; 11: 63–8.

Gloor P, Pellegrini A, Kostopoulos GK. Effects of changes in cortical excitability upon the epileptic bursts in generalized penicillin epilepsy of the cat. Electroencephalogr Clin Neurophysiol 1979; 46: 274–89.

Grady SR, Meinerz NM, Cao J, Reynolds AM, Picciotto MR, Changeux JP, et al. Nicotinic agonists stimulate acetylcholine release from mouse interpeduncular nucleus: a function mediated by a different nAChR than dopamine release from striatum. J Neurochem 2001; 76: 258–68.

Groenewegen HJ, Ahlenius S, Haber SN, Kowall NW, Nauta WJ. Cytoarchitecture and fiber connections and some histochemical aspects of the interpeduncular nucleus in the rat. J Comp Neurol 1986; 249: 65–102.

Haun F, Eckenrode TC, Murray M. Habenula and thalamus cell transplants restore normal sleep behaviors disrupted by denervation of the interpeduncular nucleus. J Neurosci 1992; 12: 3282–90.

Jones BE. The organization of central cholinergic systems and their functional importance in sleep-waking states. Prog Brain Res 1993; 98: 61–71.

Kennedy C, Gillin JC, Mendelson W, Suda S, Miyaoka M, Ito M, et al. Local cerebral glucose utilization in non-rapid eye movement sleep. Nature 1982; 297: 325–7.

Kimes AS, Horti AG, London ED, Chefer SI, Contoreggi C, Ernst M, et al. 2-[18F]F-A-85380: PET imaging of brain nicotinic acetylcholine receptors and whole body distribution in humans. FASEB J 2003; 17: 1331–3.

Kuryatov A, Luo J, Cooper J, Lindstrom JM. Nicotine acts as a pharmacological chaperone to upregulate human {alpha}4{beta}2 AChRs. Mol Pharmacol 2005; 68: 1839–51.

Lee KH, McCormick DA. Modulation of spindle oscillations by acetylcholine, cholecystokinin and 1S,3R-ACPD in the ferret lateral geniculate and perigeniculate nuclei in vitro. Neuroscience 1997; 77: 335–50.

Lena C, Changeux JP, Mulle C. Evidence for 'preterminal' nicotinic receptors on GABAergic axons in the rat interpeduncular nucleus. J Neurosci 1993; 13: 2680–8.

Leniger T, Kananura C, Hufnagel A, Bertrand S, Bertrand D, Steinlein OK. A new Chrna4 mutation with low penetrance in nocturnal frontal lobe epilepsy. Epilepsia 2003; 44: 981–5.

Marutle A, Warpman U, Bogdanovic N, Nordberg A. Regional distribution of subtypes of nicotinic receptors in human brain and effect of aging studied by (+/-)-[3H]epibatidine. Brain Res 1998; 801: 143–9.

McLellan A, Phillips HA, Rittey C, Kirkpatrick M, Mulley JC, Goudie D, et al. Phenotypic comparison of two Scottish families with mutations in different genes causing autosomal dominant nocturnal frontal lobe epilepsy. Epilepsia 2003; 44: 613–7.

Moulard B, Picard F, le Hellard S, Agulhon C, Weiland S, Favre I, et al. Ion channel variation causes epilepsies. Brain Res Brain Res Rev 2001; 36: 275–84.

Nauta WJ. Hippocampal projections and related neural pathways to the midbrain in the cat. Brain 1958; 81: 319–40.

Nguyen HN, Rasmussen BA, Perry DC. Subtype-selective up-regulation by chronic nicotine of high-affinity nicotinic receptors in rat brain demonstrated by receptor autoradiography. J Pharmacol Exp Ther 2003; 307: 1090–7.

Phillips HA, Favre I, Kirkpatrick M, Zuberi SM, Goudie D, Heron SE, et al. CHRNB2 is the second acetylcholine receptor subunit associated with autosomal dominant nocturnal frontal lobe epilepsy. Am J Hum Genet 2001; 68: 225–31.

Phillips HA, Marini C, Scheffer IE, Sutherland GR, Mulley JC, Berkovic SF. A de novo mutation in sporadic nocturnal frontal lobe epilepsy. Ann Neurol 2000; 48: 264–7.

Picard F, Bertrand S, Steinlein OK, Bertrand D. Mutated nicotinic receptors responsible for autosomal dominant nocturnal frontal lobe epilepsy are more sensitive to carbamazepine. Epilepsia 1999; 40: 1198–209.

Picard F, Scheffer I. Recently defined genetic epileptic syndromes. In: Roger J, Bureau M, Dravet C, Genton P, Tassinari CA, Wolf P, editors. Epileptic syndromes in infancy, childhood and adolescence. Montrouge: John Libbey Eurotext; 2005. p. 519–35.

Provini F, Plazzi G, Tinuper P, Vandi S, Lugaresi E, Montagna P. Nocturnal frontal lobe epilepsy. A clinical and polygraphic overview of 100 consecutive cases. Brain 1999; 122: 1017–31.

Rodrigues-Pinguet N, Jia L, Li M, Figl A, Klaassen A, Truong A, et al. Five ADNFLE mutations reduce the Ca2+ dependence of the mammalian alpha4beta2 acetylcholine response. J Physiol 2003; 550: 11–26.

Rozycka A, Skorupska E, Kostyrko A, Trzeciak WH. Evidence for S284L mutation of the CHRNA4 in a white family with autosomal dominant nocturnal frontal lobe epilepsy. Epilepsia 2003; 44: 1113–7.

Sallette J, Pons S, Devillers-Thiery A, Soudant M, Prado de Carvalho L, Changeux JP, et al. Nicotine upregulates its own receptors through enhanced intracellular maturation. Neuron 2005; 46: 595–607.

Sastry BR. Effects of substance P, acetylcholine and stimulation of habenula on rat interpeduncular neuronal activity. Brain Res 1978; 144: 404–10.

Scheffer IE, Bhatia KP, Lopes-Cendes I, Fish DR, Marsden CD, Andermann E, et al. Autosomal dominant nocturnal frontal lobe epilepsy. A distinctive clinical disorder. Brain 1995; 118: 61–73.

Schöllhorn-Peyronneau M, Coulon C, Bruel D, Ottaviani M, Valette H, Deverre JR, et al. A sensitive and specific quantification of unchanged [18F]-fluoro-A-85380 in plasma by solid phase extraction for human PET studies. Eur J Nucl Med 2005; 32: S247 [Abstract].

Smith Y, Pare D, Deschenes M, Parent A, Steriade M. Cholinergic and non-cholinergic projections from the upper brainstem core to the visual thalamus in the cat. Exp Brain Res 1988; 70: 166–80.

Steinlein OK, Mulley JC, Propping P, Wallace RH, Phillips HA, Sutherland GR, et al. A missense mutation in the neuronal nicotinic acetylcholine receptor alpha 4 subunit is associated with autosomal dominant nocturnal frontal lobe epilepsy. Nat Genet 1995; 11: 201–3.

Steinlein OK, Stoodt J, Mulley J, Berkovic S, Scheffer IE, Brodtkorb E. Independent occurrence of the CHRNA4 Ser248Phe mutation in a Norwegian family with nocturnal frontal lobe epilepsy. Epilepsia 2000; 41: 529–35.

Steriade M, Datta S, Pare D, Oakson G, Curro Dossi RC. Neuronal activities in brain-stem cholinergic nuclei related to tonic activation processes in thalamocortical systems. J Neurosci 1990; 10: 2541–59.

Takagi M. Actions of cholinergic drugs on cells in the interpeduncular nucleus. Exp Neurol 1984; 84: 358–63.

Talairach J, Tournoux P. Co-planar stereotaxic atlas of the human brain. Stuttgart: Thieme; 1988.

Tassinari C, Gardella E, Meletti S, Rubboli G. The neuroethological interpretation of motor behaviours in 'nocturnal-hyperkinetic-frontal seizures': emergence of 'innate' motor behaviours and role of central pattern generators. In: Beaumanoir A, Andermann F, Chauvel P, Mira L and Zifkin B, editors. Frontal lobe seizures and epilepsies in children. Montrouge: John Libbey Eurotext; 2003: p. 43–8.

Torrao AS, Lindstrom JM, Britto LR. Nicotine and alpha-bungarotoxin modify the dendritic growth of cholinoceptive neurons in the developing chick tectum. Brain Res Dev Brain Res 2003; 143: 115–8.

Tribollet E, Bertrand D, Marguerat A, Raggenbass M. Comparative distribution of nicotinic receptor subtypes during development, adulthood and aging: an autoradiographic study in the rat brain. Neuroscience 2004; 124: 405–20.

Valette H, Bottlaender M, Dolle F, Guenther I, Coulon C, Hinnen F, et al. Characterization of the nicotinic ligand 2-[18F]fluoro-3-[2(S)-2-azetidinylmethoxy]pyridine in vivo. Life Sci 1999a; 64: PL93–7.

Valette H, Bottlaender M, Dolle F, Guenther I, Fuseau C, Coulon C, et al. Imaging central nicotinic acetylcholine receptors in baboons with [18F]fluoro-A-85380. J Nucl Med 1999b; 40: 1374–80.

Valjakka A, Vartiainen J, Tuomisto L, Tuomisto JT, Olkkonen H, Airaksinen MM. The fasciculus retroflexus controls the integrity of REM sleep by supporting the generation of hippocampal theta rhythm and rapid eye movements in rats. Brain Res Bull 1998; 47: 171–84.

Weiland S, Witzemann V, Villarroel A, Propping P, Steinlein O. An amino acid exchange in the second transmembrane segment of a neuronal nicotinic receptor causes partial epilepsy by altering its desensitization kinetics. FEBS Lett 1996; 398: 91–6.

Williams JA, Comisarow J, Day J, Fibiger HC, Reiner PB. State-dependent release of acetylcholine in rat thalamus measured by in vivo microdialysis. J Neurosci 1994; 14: 5236–42.

Zoli M, Le Novere N, Hill JA Jr, Changeux JP. Developmental regulation of nicotinic ACh receptor subunit mRNAs in the rat central and peripheral nervous systems. J Neurosci 1995; 15: 1912–39.

Zoli M, Lena C, Picciotto MR, Changeux JP. Identification of four classes of brain nicotinic receptors using beta2 mutant mice. J Neurosci 1998; 18: 4461–72.